

A route to a more sustainable nickel composite electrodeposit, using turmeric and a new low nickel ion concentration electrolyte

Richard James Merrill, Liang Wu, John Graves, Jamie Beddow, Elena Fuentes and Andrew Cobley

Author post-print (accepted) deposited by Coventry University's Repository

Original citation & hyperlink:

Merrill, R., et al. "A route to a more sustainable nickel composite electrodeposit, using turmeric and a new low nickel ion concentration electrolyte." *Surface and Coatings Technology* (2019): 125024.

<https://dx.doi.org/10.1016/j.surfcoat.2019.125024>

ISSN 0257-8972

Publisher: Elsevier

NOTICE: this is the author's version of a work that was accepted for publication in *Surface and Coatings Technology*. Changes resulting from the publishing process, such as peer review, editing, corrections, structural formatting, and other quality control mechanisms may not be reflected in this document. Changes may have been made to this work since it was submitted for publication. A definitive version was subsequently published in *Surface and Coatings Technology*, Vol 380, (2019) DOI: [10.1016/j.surfcoat.2019.125024](https://doi.org/10.1016/j.surfcoat.2019.125024)

© 2017, Elsevier. Licensed under the Creative Commons Attribution-NonCommercial-NoDerivatives 4.0 International

<http://creativecommons.org/licenses/by-nc-nd/4.0/>

Copyright © and Moral Rights are retained by the author(s) and/ or other copyright owners. A copy can be downloaded for personal non-commercial research or study, without prior permission or charge. This item cannot be reproduced or quoted extensively from without first obtaining permission in writing from the copyright holder(s). The content must not be changed in any way or sold commercially in any format or medium without the formal permission of the copyright holders.

This document is the author's post-print version, incorporating any revisions agreed during the peer-review process. Some differences between the published version and this version may remain and you are advised to consult the published version if you wish to cite from it.

Manuscript cover

A route to a more sustainable nickel composite electrodeposit, using turmeric and a new low nickel ion concentration electrolyte

R. Merrill^{a,*}, L. Wu^a, J. E. Graves^a, J. Beddow^a, E. Fuentes^b, A. Cobley^a

^aThe Functional Materials Research Group, Institute for Future Transport and Cities, Coventry university, Priory Street, Coventry, CV1 5FB, United Kingdom

^bIK4-TEKNIKER, Parke Teknologikoa, C/Iñaki Goenaga 5, 20600 Eibar, Gipuzkoa (Spain)

Abstract: Electrodeposited nickel composites are often used as protective coatings with many important applications. The filler particles used in these composites can be expensive, requiring energy-intensive production methods to produce, whilst the composites themselves are difficult to recycle. The research aim was to use a sustainable filler particle (the spice turmeric), to produce a more sustainable electrodeposited nickel composite coating and characterise its properties. A new low nickel ion concentration electrolyte (LICE) was developed to prevent agglomeration of the turmeric particles in solution. The pure nickel deposit produced from the LICE electrolyte exhibited analogous hardness and salt spray corrosion rate to that of pure nickel deposits produced from a Watts electrolyte. The incorporation of turmeric into the nickel deposit refined the grain structure, increasing the deposit's hardness to 536 HV, its salt spray corrosion rate to 189 mm y⁻¹ and increasing the water contact angle to 104°. The hardness exhibited by the deposits at a turmeric concentration of 5.0 g/L was equal to or better than many nickel composites reported in the literature.

Keywords : Electrodeposition, nickel, corrosion, hardness, sustainable, composite

Introduction 1.

Nickel is hard, ductile, ferromagnetic up to 360 °C, highly resistant to corrosion in both water and air and resists most acids. Nickel is often used as a protective coating, having many important applications including tubing in desalination plants, aircraft turbine components, and marine petroleum and chemical processing equipment [1,2]. Electrodeposited nickel is one of the most widely used surface finishing processes in the electroplating industry, with over 150,000 tonnes of nickel being deposited globally each year [3,4]. However, for many high value applications a multi-functional coating is required, and electrodeposited single-phase nickel coatings may not possess all the desired properties. Composite coatings generally have multi-functional properties compared to their homogeneous counterparts, with modified properties that strongly depend on the nature of particles/fibres incorporated and their effects on the grain structure of the deposit [5-11]. The electrodeposition of nickel composite coatings has been extensively studied. Lubricant particles such as polytetrafluoroethylene (PTFE) have been shown to lower the coefficient of friction, and increase the water contact angle of the deposit [9,12,13]. The electrocodeposition of carbon nanotubes into a nickel matrix has been shown to reduce the grain size of the deposit and increase its hardness and wear resistance [10,14,15]. The electrocodeposition of nano-SiC particles has been shown to reduce the grain size of the deposit increasing hardness, wear resistance and corrosion resistance [16,17]. The enhancements exhibited by composites over their single-phase counterparts is not achieved without drawbacks in sustainability. Composites are extremely difficult to recycle due to their inherent heterogeneous nature, and the particles electrocodeposited can be expensive and require energy intensive methods to produce [18]. The development of a nickel electrodeposited composite coating from a sustainably sourced particle would therefore be of great academic and industrial interest.

One possible source of sustainable particles may be herbs and spices. Herbs and spices have had many applications throughout history from flavour enhancers and medicines to currency [19]. Turmeric has received a great deal of scientific interest in recent years due to its medicinal properties, however its properties as a sustainable filler particle for composites has not been studied [20-23].

The aim of this research was to develop a more sustainable nickel electrocodeposited composite. This paper describes for the first time the codeposition of turmeric particles into a nickel deposit produced from a new low nickel ion concentration electrolyte, and the characterisation of these deposits.

2.1. Materials and method

Nickel samples were electrodeposited under direct current conditions (DC) at a current density of 0.04 A/cm^2 and temperature of $50 \text{ }^\circ\text{C}$. An average deposit thickness of $30 \text{ }\mu\text{m}$ was achieved using a plating time of 37.5 min. The electrolytes were stirred throughout deposition using a $35 \times 8 \text{ mm}$ PTFE magnetic stirring bar at a speed of 200 rpm. Although low metal ion concentration electrolytes can exhibit reduced limiting cathodic current density, the use of a new low nickel ion concentration electrolyte (LICE) was necessary to prevent the agglomeration of turmeric particles. The LICE electrolyte was an aqueous solution with a Ni ion concentration of 0.58 mol/L , and consisted of $105.0 \pm 1.0 \text{ g/L}$ $\text{NiCl}_2 \cdot 6\text{H}_2\text{O}$ supplied by Alfa Aesar, $40.0 \pm 1.0 \text{ g/L}$ $\text{NiSO}_4 \cdot 6\text{H}_2\text{O}$ supplied by BDH chemicals Ltd, and $40.0 \pm 1.0 \text{ g/L}$ H_3BO_3 (>99.5%) Supplied by Sigma Aldrich UK Ltd, at pH 3.0-3.5. Deposits produced from the LICE electrolyte were compared to a control deposit produced from a Watts electrolyte (commonly used throughout industry and academia). The Watts electrolyte was an aqueous solution with a Ni ion concentration of 1.06 mol/L and consisted of $250.0 \pm 1.0 \text{ g/L}$ $\text{NiSO}_4 \cdot 6\text{H}_2\text{O}$, $50.0 \pm 1.0 \text{ g/L}$ $\text{NiCl}_2 \cdot 6\text{H}_2\text{O}$, and $40.0 \pm 1.0 \text{ g/L}$ H_3BO_3 (>99.5%), at pH 3.0-3.5. The experimental setup is illustrated in Fig 1. Although, surfactants introduce environmental

problems such as toxicity to aquatic organisms [24], the use of the non-ionic surfactant Tween 20 was necessary to help prevent re-agglomeration of the turmeric particles in the LICE electrolyte. Between 1.0 and 10.0 g/L of turmeric supplied by Healthy Supplies UK Ltd was added to the LICE electrolyte, with 10.0 ml/L of the non-ionic surfactant Tween 20 ($C_{58}H_{114}O_{26}$) supplied by Sigma Aldrich UK Ltd. The turmeric was a pre-ground powder, with a particle size distribution of 90 - 2500 nm and a mean particle size of 1082 ± 310 nm. The turmeric particles were dispersed before deposition by ultrasound from a 20 kHz Sonic Systems sonic processor P100/3-20 horn model GA99893 for 20 min at a power of 11 W/L (measured by calorimetry). A 0.9 mm thick brass sheet with a plating area of 25 mm^2 was used as the cathode, a pure nickel sheet of equal dimensions was used as the anode. Both cathode and anode were submerged in an aqueous solution of 10 % Decon supplied by Sigma Aldrich UK Ltd, at ambient room temperature for 60 s to remove any surface contaminants. The oxidation layers were removed by submersion in a 3.9 M solution of H_2SO_4 at ambient room temperature for 60 s. The cathode and anode were then rinsed with DI water and immediately placed in the electrolyte.

2.2. Microstructure

Carbohydrates ($(CH_2O)_n$) are the major component of turmeric at 67 %, other organic compounds are also present (such as proteins, fats, essential oils, and curcuminoids) [25,26]. The carbon content of the composites was examined at the centre of the deposits, with a GD Profiler 2 (HORIBA Jobin Yvon) RF Glow Discharge Optical Emission Spectrometer (GDOES) to assess the successful incorporation of turmeric. The GDOES data was then compared to a control sample, produced from the same LICE electrolyte but with the absence of turmeric (LICE electrolyte containing only Tween 20). Microstructure analysis was performed to assess the effect of turmeric on the grain structure of the deposits. High-resolution images of the surface of the deposit were obtained using a Zeiss sigma 500 VP scanning electron microscope (SEM). Grain structure data was obtained using an oxford

instruments AZtec electron backscatter detector (EBSD), at 20 kV and stepping size of 33 nm. The deposits were cross-sectioned and mounted in PolyFast Struers resin for hot mounts, then ground with successively finer grit sanding discs until only small parallel scratch marks were visible. The final polish was performed with OP-S 0.04 μm solution. High-resolution images of the cross-section of the deposits were obtained using an FEI versa 3D FIB-SEM focused ion beam scanning electron microscope. ImageJ software was used to examine the Ion beam images and calculate the grain size using the line intercept method [27].

$$Gs = \frac{l}{n} \quad (1)$$

Where Gs is the grain size in nm, l is the line length in nm, and n is the number of grains that intercept the line.

2.3. Properties

Hydrophobic behaviour, hardness and corrosion resistance were examined to quantify the enhancements the incorporation of turmeric imparted on the deposits. The hydrophobic behaviour was assessed by measuring the water contact angle (WCA), with a Kruss DSA 100 drop shape analysis system. A droplet of 2.0 μl of DI water was placed at 6 random positions on the surface of the deposits, 3 separate deposits were used for each sample set and the mean calculated. The deposits hardness was measured using a Mitutoyo MVK-H1 microhardness tester, with a Vicker's indenter. Each deposit was indented at 7 random positions, 3 separate deposits were used for each sample set and the mean calculated. The average surface roughness (R_a) of the deposits was measured using a Bruker contour GT white light interferometer (WLI). Measurements were taken at random positions on each sample, and the mean calculated from 3 separate deposits of the same sample set. Both electrochemical and salt spray methods were used to assess the corrosion rate. The electrochemical corrosion rate was calculated from the extrapolation of the Tafel region of the potentiodynamic curve. A

VoltaLab PST 050 potentiostat was connected to a 3-electrode cell with a Pt counter electrode (CE) a Hg/Hg₂Cl₂ sat. KCl reference electrode (RE) and the sample as the working electrode (WE). An exposure area of 10 mm² at the centre of the deposit was obtained for testing by applying chemical resistant tape. A 0.1 M electrolyte solution of Na₂SO₄ was used. The open circuit potential (OCP) was measured, and the potential swept linearly from -200 mV of the OCP to +200 mV of the OCP in steps of 0.1 mV/s. The log(*i*) vs *E* curves were plotted, and corrosion current (*i*_{corr}) obtained at the corrosion potential (*E*_{corr}). The *i*_{corr} was used to calculate the corrosion rate (*C*_R) using equation 2.

$$C_R = \frac{i_{corr} k Z}{d A n} \quad (2)$$

Where *k* is the constant that defines the units of the corrosion rate (3272 mm/y⁻¹), Where *z* is the atomic mass of Ni, *d* is the density of the material deposited in g/cm³ (8.91 g/cm³), *A* is the surface area in cm² (1 cm²), and *n* is the electron stoichiometry. The salt spray corrosion rate was measured using an Ascott cc ip 1000 salt spray chamber. The method used was adapted from ASTM B 117 – 03, Standard Practice for Operating Salt Spray (Fog) Apparatus. A solution of 5.0 % wt NaCl was used, each deposit was pre-weighed and placed in the salt spray chamber for 240 hours, the deposits were then washed with deionised water, dried and re-weighed. The mass lost was used to calculate the corrosion rate using equation 3.

$$C_R = \frac{k W}{A t d} \quad (3)$$

Where *k* is a constant that defines the units of the corrosion rate (3.45e⁶ m/year), *W* is the mass lost in g, *A* is the area exposed to the salt spray in cm² (2.5 cm²), *t* is time in hours, and *d* is the density of nickel.

3. Results and discussion

3.1 Dispersion

Fig 2. shows a significant reduction in turmeric on the surface of the LICE electrolyte compared to the Watts electrolyte. The substantial amount of turmeric observed on the surface of the Watts electrolyte made the deposition of good quality turmeric composites problematic. The agglomeration of the turmeric particles may have been due to several factors. The ionic strength of an aqueous electrolyte is known to affect the interaction of particles in solution. Charge density and ionic concentration can increase the tendency of hydrophobic particles to aggregate, becoming significant at moderate ion concentrations (0.1-1.0 M) in a process known as salting out [28-31]. The charge and zeta potential of a particle in solution can also be influenced by the ionic strength of an electrolyte; which can affect the dispersion of the particles [32,33]. A decrease in the zeta potential or particle charge can result in reduced repulsion between particles and increased agglomeration [34,35].

3.2 Surface finish

Fig 3. shows both the pure Watts and LICE deposits exhibited analogous matte grey finish. Although small pits were present at the edge of both samples, fewer pits were visible in the deposit produced from the LICE electrolyte. The addition of 10.0 ml/L of Tween 20 to the LICE electrolyte resulted in a deposit with the brightest finish and no visible pits. The further addition of turmeric to the LICE electrolyte resulted in dulling of the deposits. All deposits showed some edge build-up, caused by the current at the edges of the cathode being higher than the centre [36,37]. The pits present in the pure nickel deposits were likely due to the formation of $H_{2(g)}$ on the surface of the cathode. The discharge of $H_{2(g)}$ at the cathode is typical in nickel electrodeposition, usually consuming a small amount of current [38]. The lack of pits seen in the deposits containing Tween 20 can be attributed to the presence of a surfactant in the electrolyte. Surfactants can modify the grain structure of a deposit and act as brighteners. Brighteners can increase the nucleus density of newly formed nuclei and increase the rate of hydrogen desorption from the cathode [39-44]. The presence of the surfactant in the electrolyte is also likely responsible for the bright finish exhibited by the LICE deposit

containing just Tween 20. The modifying effect of Tween 20 on the grain structure of the deposit enhanced the deposit's smoothness, increasing its brightness [45,45]. The progressive decrease in brightness thereafter is likely due to an increase in the surface roughness caused by the incorporation of turmeric.

3.3. Microstructure

The GDOES results presented in Fig 4. show a large spike in carbon content at the surface of the deposits, which can be attributed to organic surface contaminants. All deposit showed a thickness of less than 30 μm at their centre, which was due to the uneven current distribution on the cathode. A progressive increase in carbon content was observed from the LICE deposit containing just Tween 20, to the deposit containing 10.0 g/L of Turmeric. Past research has shown additives such as surfactants and inert particles can be incorporated into electrodeposited nickel when present in the electrolyte [45-47]. Particles are transported to the cathode by a combination of electrophoresis, convection, and diffusion; whereupon they are absorbed and entrapped in the growing electrodeposit [48]. The carbon content observed in the LICE deposit containing just Tween 20 was due to the incorporation of the surfactant, whereas the carbon content in the composite deposits was due to the incorporation of both Tween 20 and turmeric. The same Tween 20 concentration was utilised for all deposits; however, the turmeric electrolyte concentration was varied, this suggests that the increase in carbon content in the composite deposits was due to the increase in turmeric electrolyte concentration. This is consistent with past research which has shown increasing electrolyte particle concentration generally results in an increase in deposit particle content until a saturation point is reached [9,49-51].

High magnification SEM images of the nickel deposits are presented in Fig 5. The SEM images show the two pure nickel deposits exhibited different crystal morphology. The literature shows that comparing the surface morphology of a deposit to one with a known

crystallographic orientation allows high magnification SEM images to be used to assess crystallographic orientation [52]. Although both deposits exhibited pyramidal structure, clear variations were observed, with the pure nickel deposited from the LICE electrolyte exhibiting sharper more angular grains. The electrocrystallisation of nickel is known to be a highly inhibited process due to hydrogen co-deposition [52-54]. Nickel deposited from Watts type electrolytes display 3 inhibited textures ([110], [210] and [211]) due to the presence of both atomic and molecular forms of absorbed and colloidal hydrogen in the cathodic interface [52-55]. The literature shows increasing the Cl^- ion concentration in a Watts type electrolyte changes the preferred crystallographic orientation from [110] to [211], and increasing the SO_4^{2-} ion concentration changes the preferred crystallographic orientation from [110] to [210], then back again to [110] with further increases [56]. The deposit produced from the LICE electrolyte containing just Tween 20, exhibited finer grains compared to the pure nickel deposits, however, microcracks were observed. The presence of microcracks in the deposit is likely due to increased intrinsic stress. The incorporation of a surfactant into a nickel electrodeposit is known to modify the grain structure, which can induce excessive brittleness and increase stress [45-47]. Stress can also be induced after deposition by thermal expansion, mismatch between substrate and coating, or grain growth if the deposit possesses sufficient atomic mobility. Microcracks can occur as a result of the release of built-up stress in the electrodeposit [47,57]. A progressive increase in nodulation was observed with increasing electrolyte turmeric concentration. The observed nodulation was likely due to the co-deposition of turmeric into the deposit. Nodules are common in nickel deposits and can be caused by the incorporation of inert particles, resulting in an uneven current distribution on the cathode. [58-61]. No microcracks were observed in the deposits containing turmeric, suggesting the absence of intrinsic stress or a significant reduction. The co-deposition of inert particles into a deposit is also known to refine the grain structure without introducing the intrinsic stress caused by surfactants alone [57,62].

EBSD maps of the electrodeposits are presented in Fig 6. Ion beam images obtained by FIB-SEM are presented in Fig 7. and grain size data generated by EBSD and the line intercept method is presented in Table 2. Both the EBSD maps and the ion beam images showed both pure nickel deposits exhibited analogous grain structure, showing similar size grains of mainly columnar crystals with high aspect ratios. The inverse pole figure colour key showed clear differences in the preferred crystallographic orientation between the samples, which was consistent with observations made from the SEM images. EBSD data for deposits containing turmeric could not be obtained. Which may be due to several factors, the polishing method was insufficient to reduce the roughness, the presence of material in the deposit not detectable by EBSD (such as turmeric), amorphous deposits or with a grain size smaller than the minimum stepping size of the EBSD detector (33 nm). The small concentration of turmeric in the deposit is unlikely to result in large areas being undetectable by EBSD, however, the presence of turmeric may have made the polishing method insufficient. Ion beam images showed analogous grain structure was exhibited by the LICE deposit containing only Tween 20 and the LICE deposit containing 1.0 g/L of turmeric (which was significantly finer than either pure nickel deposits). The size of grains exhibited by these deposits was within error of the minimum stepping size of the EBSD detector, which is likely responsible for the lack of EBSD data obtained. The significant change in grain structure observed in the LICE deposit containing only Tween 20 was due to the incorporation of the surfactant into the deposit. Surfactants can be incorporated into an electrodeposit when present in the electrolyte, modifying the deposits grain structure [41,44,63]. The significant effect of Tween 20 on the grain structure of the deposit was responsible for the lack of visual change in grain structure on the addition of 1.0 g/L of turmeric. Although the incorporation of inert particles into an electrodeposit can refine its grain structure [64,65], the addition of a small amount of turmeric thereafter was not sufficient to further reduce the grain size. A further significant change in grain structure was observed with an increase in turmeric concentration to 5.0 g/L. No

individual grains could be identified in the LICE deposits produced from 5.0 g/L or 10.0 g/L of turmeric, giving the deposits an amorphous-like appearance. This suggests that the deposits either exhibited grains too small to be identified or the deposits were amorphous. The lack of EBSD data generated for these two deposits is, therefore, likely due to the samples exhibiting a grain size smaller than 33 nm or the deposits being amorphous. The significant change in grain structure observed when the electrolyte turmeric concentration was increased from 1.0 g/L to 5.0 g/L shows that the presence of turmeric had a significant refinement effect on the grain structure of the deposit. However, the additional increase in turmeric electrolyte concentration from 5.0 g/L to 10.0 g/L had no further effect, as the maximum grain structure modification possible had already been achieved.

3.4. Properties

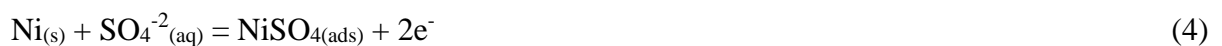
Hardness values for the nickel deposits are presented in Fig 8. The pure nickel deposits produced from the Watts and LICE electrolyte exhibited similar hardness. A significant enhancement in hardness was exhibited with the addition of 10.0 ml/L of Tween 20 to the LICE electrolyte, the further addition of 1.0 g/L of turmeric did not result in increased hardness. A significant increase in hardness was observed when the turmeric electrolyte concentration was increased to 5.0 g/L. Although increasing the electrolyte turmeric concentration thereafter to 10.0 g/L resulted in a small reduction in hardness, this was within error of the deposit produced from 5.0 g/L of turmeric. The extent of the increase in hardness observed with the addition of 5.0 g/L of turmeric was greater than that reported in the literature for WC, SiC, MWCNT, graphene, and alumina particles (Fig 9.) [66-73]. The change in grain structure was responsible for the enhanced hardness exhibited by the deposits containing Tween 20 and turmeric. Grain size is a major factor influencing the hardness of an electrodeposit [40,74-84]. The number of grain boundaries increases as the grain size is reduced. When sufficient force is applied to the deposit, dislocations build-up at grain boundaries, either because a barrier to crossing over exists, or a source must be activated in

the next grain boundary. A specific concentration for a given grain is required to initiate slip into the neighbouring grain boundary. This concentration is most likely achieved through a dislocation build-up. Stress is higher as the number of dislocations increases; the more substantial the grain size the quicker the stress is reached. However, this is only true at low temperatures where creep due to plastic deformation is irrelevant [80,83,84].

The data presented in Fig 10. shows the average surface roughness (Ra) of the nickel deposits obtained by White Light Interferometry (WLI). Similar Ra values were exhibited by both pure nickel deposits. The addition of 10.0 ml/L of Tween 20 to the LICE electrolyte resulted in a reduction in Ra value, which was due to grain structure refinement. A progressive increase in Ra was observed with increasing turmeric electrolyte concentration thereafter, which was due to increased surface nodulation. The increased Ra values associated with the deposits containing turmeric may adversely affect their tribological properties. An increase in Ra reduces the real area of contact between two surfaces, increasing both local contact pressures and temperatures [85]. This results in increased friction and likely wear rate when in contact with another surface if a sliding force is applied [86].

The water contact angles (WCA) of the nickel deposits are presented in Fig 11. Both the pure nickel deposits and the LICE deposit containing 10.0 g/L of Tween 20, exhibited wetting behaviour (WCA $<90^\circ$). The pure nickel Watts deposit and the LICE deposit containing only Tween 20 exhibited similar WCA. The deposits containing turmeric all exhibited non-wetting behaviour ($>90^\circ$), with similar WCA. The surface energy is the primary factor influencing the WCA of a deposit, with higher surface energy deposits having lower WCA [87-89]. Many factors can influence the surface energy of a deposit including particle content, grain size, crystallographic orientation, and surface roughness, with the change in WCA observed in this research being a combination of all these factors [89-92].

Fig 12. displays a single Tafel plot for each deposit. The mean corrosion currents (i_{corr}) generated from multiple Tafel plots for each deposit are presented in table 3. With the electrochemical corrosion rate calculated from i_{corr} presented in Fig 13. Uniformed corrosion was assumed for all deposits. The pure LICE nickel deposit exhibited a higher electrochemical corrosion rate when compared to that of the Watts deposit. The Addition of 10.0 ml/L of Tween 20 to the LICE electrolyte resulted in a deposit with the highest electrochemical corrosion rate. The inclusion of 1.0 g/L of turmeric thereafter resulted in a small decrease in I_{corr} and corrosion rate. However, a significant reduction was observed with an increase in turmeric concentration to 5.0 g/L, further increasing turmeric concentration resulted in a small increase in corrosion rate. Large variation was observed in i_{corr} and corrosion rates (with overlapping error) for some deposits, indicating a large degree of deviation in the corrosion properties between individual deposits within the same samples set. A possible mechanism for the corrosion of nickel in Na_2SO_4 has been proposed in the literature. The sulphate anion (SO_4^{-2}) is produced by the disassociation of Na_2SO_4 , and at low anodic potentials is adsorbed onto the surface of the nickel electrode (equation 4). At positive potentials, dissociated species are generated by the breakdown of the absorbed sulphate layer (equation 5) [93,94].



Differences in the surface morphology between the two pure nickel deposits would result in differences between their adsorption and dissociation rate, which is likely responsible for the divergence of their corrosion rate. The presence of microcracks in the surface of the deposit produced from the LICE electrolyte containing 10.0 ml/L of Tween 20, would allow deeper penetration of the electrolyte into the deposit resulting in increased corrosion. A combination of grain size reduction and absence of microcracks thereafter is likely responsible for an increase in the corrosion resistance exhibited by the deposits containing turmeric.

Photographic images of the nickel deposits before and after salt spray analysis are presented in Fig 14. with the corrosion rate calculated from weight loss presented in Fig 15. Uniformed corrosion was assumed for all deposits. Visual inspection after 24 hours showed a loss of lustre for the pure nickel deposits and the deposit produced from the LICE electrolyte containing only Tween 20. The pattern exhibited by the deposit produced from the LICE electrolyte containing only Tween 20 was due to how the salt solution ran off its surface. Little visual difference could be seen in the deposits containing turmeric after 24 hours. After 240 hours, only the deposits produced from the LICE electrolyte containing only Tween 20 and the deposit produce from the LICE electrolyte containing 5.0 g/L of turmeric exhibited any further visual difference, with the deposits produce from the electrolyte containing 5.0 g/L of turmeric appearing brighter after 240 hours than at the start of the experiment. This may have been due to the preferential corrosion of surface nodules increasing the smoothness of the deposit. The anodic and cathodic corrosion half cells for nickel are presented in equation 6 and 7 respectively. Little self-ionisation takes place in pure water, resulting in relatively slow corrosion. However, the addition of $\text{Na}^+ \text{Cl}^-$ increases the conductivity of the solution, significantly increasing corrosion rate [93,95].



The salt spray corrosion rate of the two pure nickel deposits was similar. Both the deposits produce from the LICE electrolyte containing only Tween 20 and 1.0 g/L of turmeric showed a significant reduction in corrosion rate when compared to the two pure nickel deposits. The deposits produced from the increased addition of 5.0 g/L and 10.0 g/L of turmeric exhibiting a further significant reduction in corrosion rate (a seven-fold decrease compared to the pure nickel deposits). The reduction in salt spray corrosion rate shows a strong correlation to the grain structure of the deposits. When exposed to air the surface of a metal is covered by an oxide film. In metals such as nickel, the oxide film serves as a protective layer (passivation

layer). Once exposed to an aqueous solution the oxide film may start to dissolve exposing the bare metal surface (known as an active state). Oxide films tend to be thinner and exposed first at grain boundaries and particle incursions. An increase in corrosion rate is observed in active systems with an increase in particle incursions or a decrease in grain size. Oxide films are less soluble in near neutral solutions, and if inhibiting ions are present the solubility may be suppressed further. Although oxide films form more rapidly on surfaces exhibiting smaller grains, oxide films are more stable on surfaces with larger grains. In a passive environment, a reduction in grain size decreases the corrosion rate.

The disparity between the corrosion rates measured by Tafel extrapolation and weight loss due to salt spray corrosion is not unexpected, and due to several factors. Although surface morphology, grain size, and porosity influence the corrosion rate of a material, the electrolyte is the primary factor [43,96,97]. Different electrolytes were used for measurements of the electrochemical corrosion rate and salt spray corrosion rate. The corrosion rate calculated by Tafel extrapolation is an estimation based on the extrapolation of the linear regions of the Tafel plot, whereas the corrosion rate calculated from the salt spray is the weight loss due to corrosion [98,99]. The microcracks in the deposit produced from the LICE electrolyte containing only Tween 20, maybe more accessible when fully submerged in the electrolyte than when exposed to the salt spray.

Conclusions

The microstructure and properties of LICE deposits containing varying amounts of turmeric were studied and compared to that of a pure nickel deposit produced from a Watts electrolyte. It was found that a uniform turmeric dispersion and good quality nickel deposits can be achieved when using the LICE electrolyte. The pure nickel deposit produced from the LICE electrolyte exhibited analogous grain size, hardness and salt spray corrosion rate to that of the deposit produce from the Watts electrolyte, however, differences in crystallographic orientation, electrochemical corrosion rate, and WCA were observed. The addition of Tween

20 to the LICE electrolyte significantly affected the deposit's microstructure and properties, reducing grain size and increasing both hardness and salt spray corrosion resistance. However, the presence of Tween 20 also induced microcracking in the deposit (likely due to increased intrinsic stress), resulting in an increased electrochemical corrosion rate. The amount of turmeric incorporated into the deposits and the properties of the deposits depended on the electrolyte turmeric concentration. The addition of a small amount of turmeric (1.0 g/L) to the electrolyte did not result in a significant change in grain size, hardness or salt spray corrosion rate, however, a small reduction was observed in the electrochemical corrosion rate, this was likely due to the absence of microcracks. At a turmeric electrolyte concentration of 5.0 g/L, the deposit produced showed a significant change in microstructure, having an amorphous like appearance or grains too small to be identified. The change in microstructure resulted in a significant increase in hardness and WCA and a significant reduction in both electrochemical and salt spray corrosion rate. Although an increase in electrolyte turmeric concentration to 10.0 g/L did show a small increase in turmeric content in the deposit, no significant change was observed in the microstructure and properties. These results show that not only is turmeric a viable sustainable alternative to some of the more commonly used filler particles, but that the extent of the increase in hardness at such a low particle cost, may make it superior to WC, SiC, MWCNT, graphene and alumina particles for increasing the hardness of a nickel deposit [66-73]. However, all nickel turmeric deposits exhibited a significant increase in surface roughness, which could result in poor tribological properties.

Table 1. Nickel samples electrodeposited from the electrolytes.

Sample	Electrolyte	Tween 20 concentration ml/l	Turmeric concentration g/L	Sample description
A	Watts	0	0	Pure Ni Watts
B	LICE	0	0	Pure Ni LICE
C	LICE	10	0	Ni LICE Tween 20
D	LICE	10	1.0	Ni LICE 1.0 g/L Turmeric
E	LICE	10	5.0	Ni LICE 5.0 g/L Turmeric
F	LICE	10	10.0	Ni LICE 10.0 g/L Turmeric

Table 2. Mean grain size of deposits obtained from EBSD and line intercept method. (A) Watts Ni. (B) LICE Ni. (C) LICE Ni Tween 20. (D) LICE Ni 1.0 g/L turmeric. (E) LICE Ni 5.0 g/L turmeric. (F) LICE Ni 1.0 g/L turmeric.

Sample	EBSD data		Line intercept data	
	Grain size y-axis nm	Grain size x-axis nm	Grain size y-axis nm	Grain size x-axis nm
A	748 ± 56	473 ± 5	887 ± 47	456 ± 23
B	811 ± 6	305 ± 68	742 ± 47	378 ± 43
C	Not detected	Not detected	66 ± 50	92 ± 50
D	Not detected	Not detected	58 ± 50	72 ± 50
E	Not detected	Not detected	Not detected	Not detected
F	Not detected	Not detected	Not detected	Not detected

Table 3. Mean i_{corr} value obtained from Tafel plots. (A) Watts Ni. (B) LICE Ni. C) LICE Ni Tween 20. (D) LICE Ni 1.0 g/L turmeric. (E) LICE Ni 5.0 g/L turmeric. (F) LICE Ni 10.0 g/L turmeric.

Samples	A	B	C	D	E	F
$i_{\text{corr}} / \text{A cm}^{-2}$	1.57×10^{-6}	2.87×10^{-6}	5.03×10^{-6}	4.01×10^{-6}	1.19×10^{-6}	1.61×10^{-6}

Fig 1. The experimental set up during electrodeposition.

Fig 2. Top view of beakers containing Watts and LICE electrolytes. (A) Watts electrolyte with 10.0 g/L of turmeric and 10.0 ml/l of Tween 20. (B) LICE electrolyte with 10.0 g/L of turmeric and 10.0 ml/l of Tween 20.

Fig 3. Photographic images of surface of nickel coatings. (A) Watts Ni. (B) LICE Ni. (C) LICE Ni Tween 20. (D) LICE Ni 1.0 g/L turmeric. (E) LICE Ni 5.0 g/L turmeric. (F) LICE Ni 10.0 g/L turmeric.

Fig 4. Coating composition obtained by GDOES. (A) LICE Ni Tween 20. (B) LICE Ni 1.0 g/L turmeric. (C) LICE Ni 5.0 g/L turmeric. (D) LICE Ni 10.0 g/L turmeric.

Fig 5. SEM images of the surface of electrodeposited nickel coatings. (A) Watts Ni. (B) LICE Ni. (C) LICE Ni Tween 20. (D) LICE Ni 1.0 g/L turmeric. (E) LICE Ni 5.0 g/L turmeric. (F) LICE Ni 10.0 g/L turmeric.

Fig 6. EBSD maps of nickel coatings electrodeposited from the following electrolytes. (A) Watts Ni. (B) LICE Ni. (C) LICE Ni Tween 20. (D) LICE Ni 1.0 g/L turmeric. (E) LICE Ni 5.0 g/L turmeric. (F) LICE Ni 10.0 g/L turmeric. (G) Inverse pole figure colour key.

Fig 7. Ion beam images of the cross section of the electrodeposited nickel coatings. (A) Watts Ni. (B) LICE Ni. (C) LICE Ni Tween 20. (D) LICE Ni 1.0 g/L turmeric. (E) LICE Ni 5.0 g/L turmeric. (F) LICE Ni 10.0 g/L turmeric.

Fig 8. Mean hardness of nickel deposits measure with a Vicker's indenter. (A) Watts Ni. (B) LICE Ni. C) LICE Ni Tween 20. (D) LICE Ni 1.0 g/L turmeric. (E) LICE Ni 5.0 g/L turmeric. (F) LICE Ni 10.0 g/L turmeric.

Fig 9. Comparison of the increase in hardness exhibited by a nickel deposit with the incorporation of various filler particles. (A) LICE Ni 5.0 g/L turmeric. (B) Ni WC [66,67]. C) Ni SiC [65,68]. (D) Ni MWCNT [69]. (E) Ni graphene [5]. (F) Ni Alumina [70,71,100].

Fig 10. Average surface roughness (Ra) of the nickel deposits measure by WLI. (A) Watts Ni. (B) LICE Ni. C) LICE Ni Tween 20. (D) LICE Ni 1.0 g/L turmeric. (E) LICE Ni 5.0 g/L turmeric. (F) LICE Ni 10.0 g/L turmeric.

Fig 11. Mean WCA of the nickel deposits. (A) Watts Ni. (B) LICE Ni. C) LICE Ni Tween 20. (D) LICE Ni 1.0 g/L turmeric. (E) LICE Ni 5.0 g/L turmeric. (F) LICE Ni 10.0 g/L turmeric.

Fig 12. Tafel plots for nickel deposits (A) Watts Ni. (B) LICE Ni. C) LICE Ni Tween 20. (D) LICE Ni 1.0 g/L turmeric. (E) LICE Ni 5.0 g/L turmeric. (F) LICE Ni 10.0 g/L turmeric.

Fig 13. Corrosion rate of nickel deposits calculate from the mean i_{corr} . (A) Watts Ni. (B) LICE Ni. C) LICE Ni Tween 20. (D) LICE Ni 1.0 g/L turmeric. (E) LICE Ni 5.0 g/L turmeric. (F) LICE Ni 10.0 g/L turmeric.

Fig 14. Photographic images of Ni deposits before and after salt spray analysis. (A) Watts Ni. (B) LICE Ni. C) LICE Ni Tween 20. (D) LICE Ni 1.0 g/L turmeric. (E) LICE Ni 5.0 g/L turmeric. (F) LICE Ni 10.0 g/L turmeric.

Fig 15. Corrosion rate of Ni coatings measure by salt spray analysis after 240 hours. (A) Watts Ni. (B) LICE Ni. C) LICE Ni Tween 20. (D) LICE Ni 1.0 g/L turmeric. (E) LICE Ni 5.0 g/L turmeric. (F) LICE Ni 10.0 g/L turmeric.

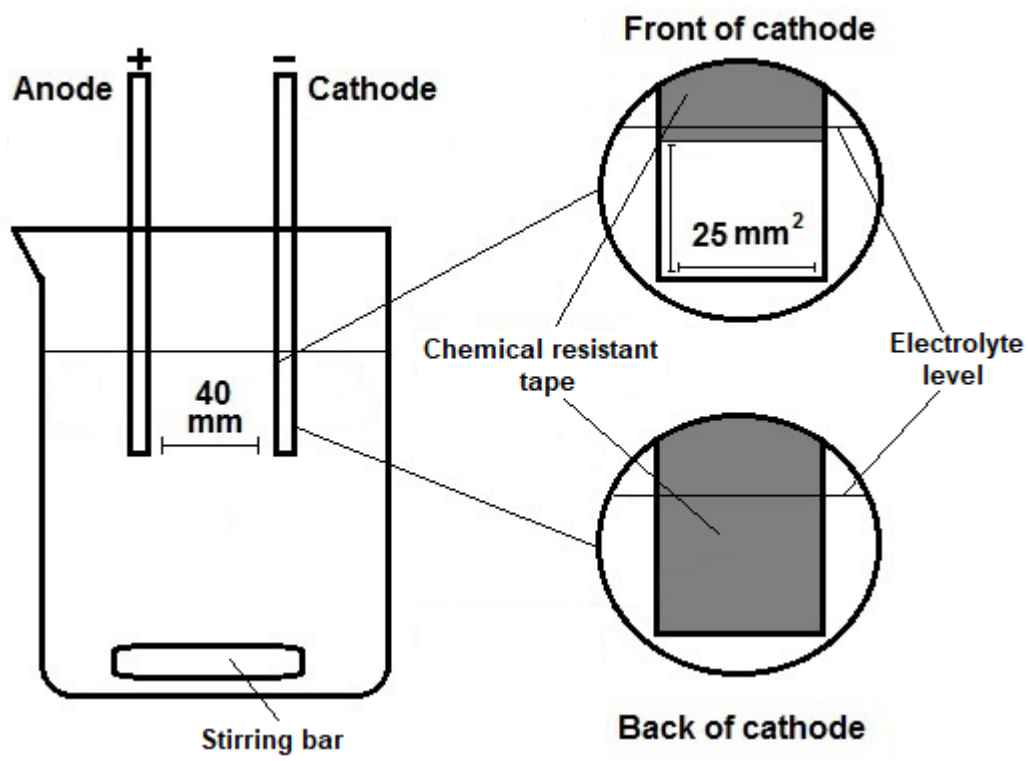


Fig 1.

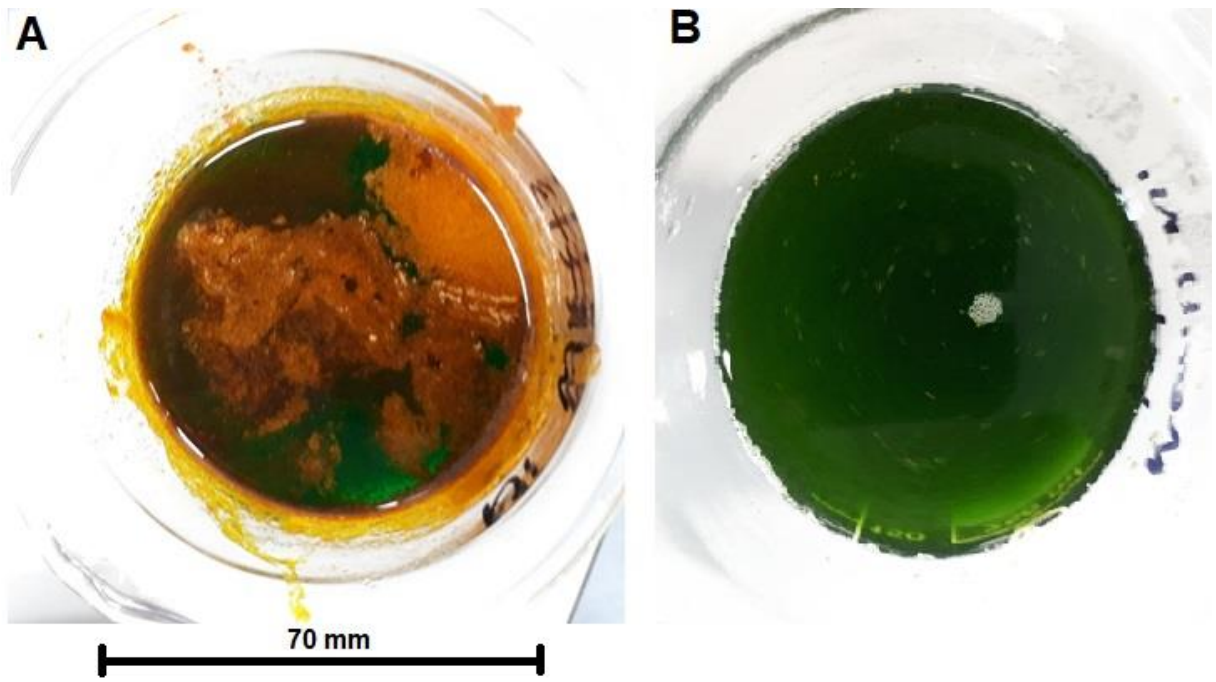


Fig 2.

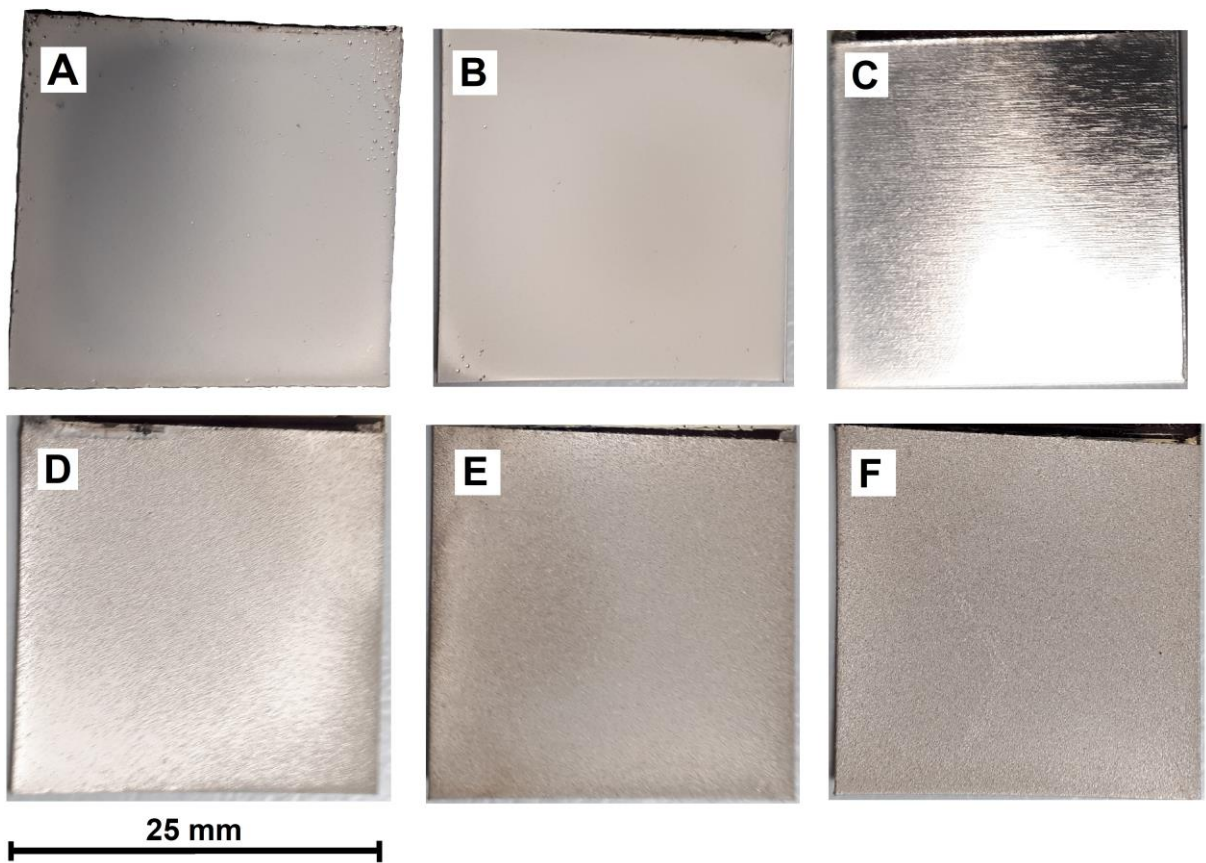


Fig 3.

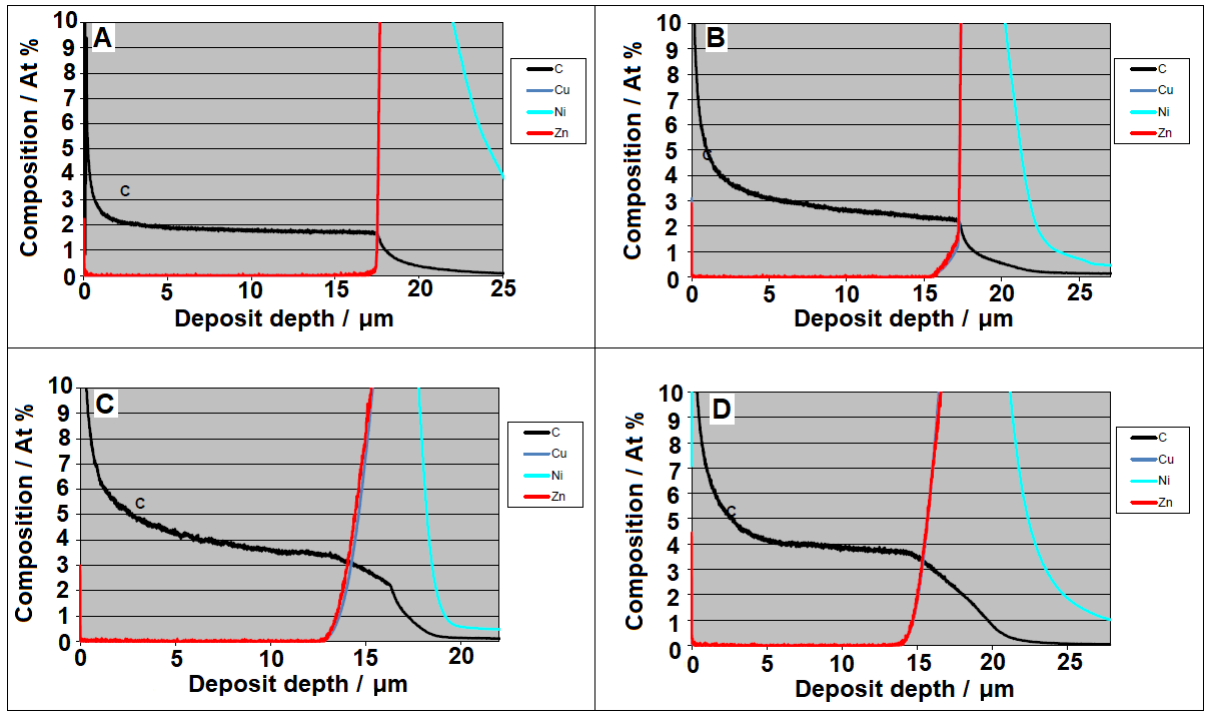


Fig 4.

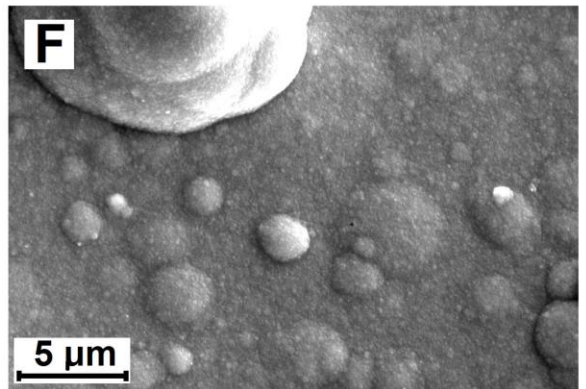
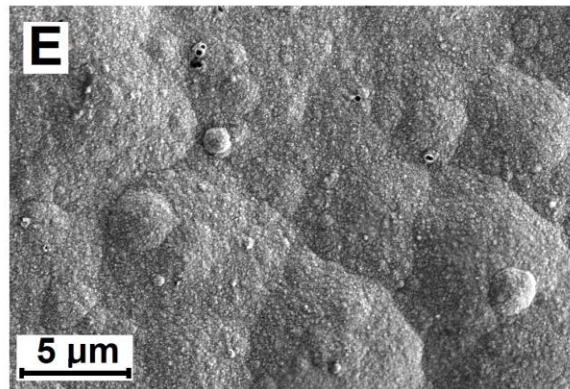
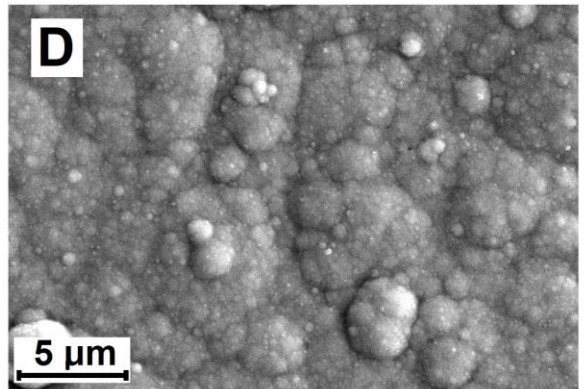
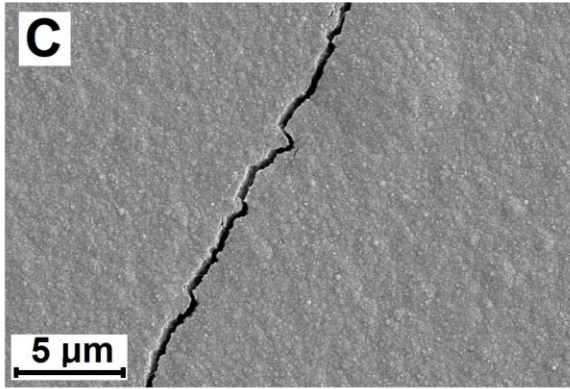
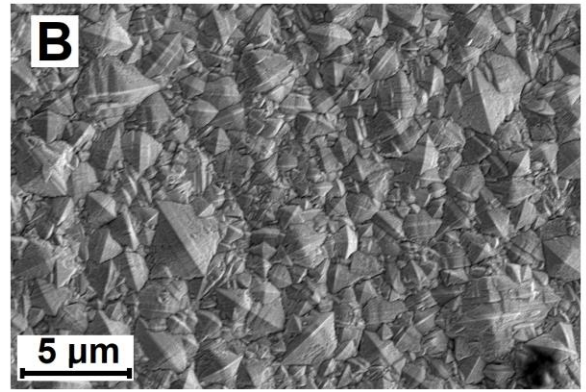
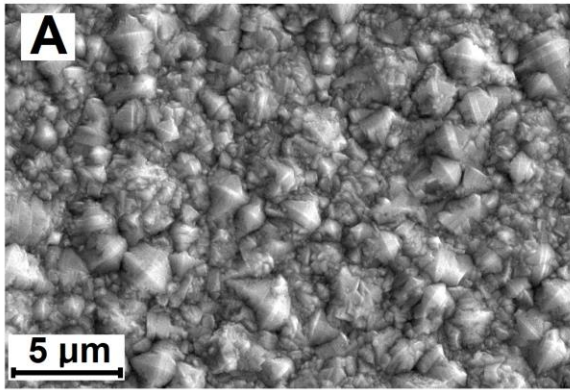


Fig 5.

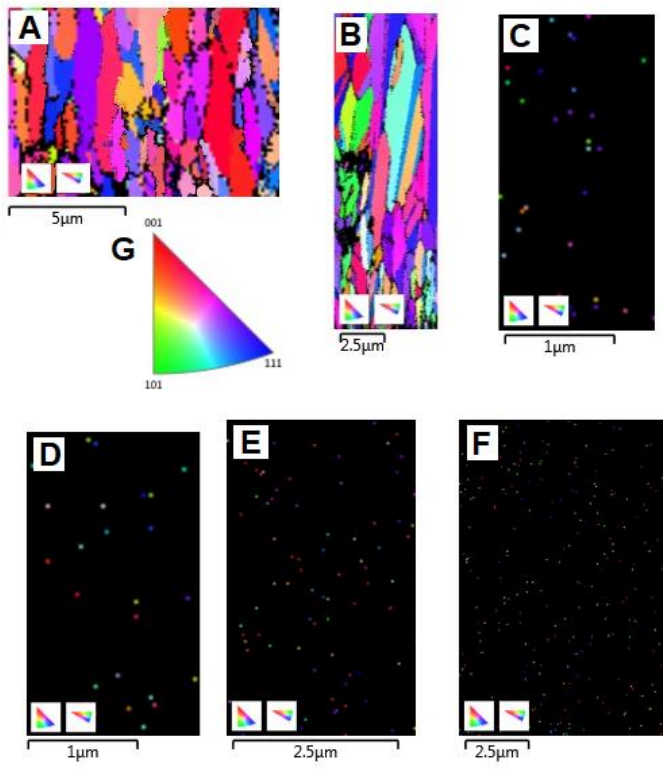


Fig 6.

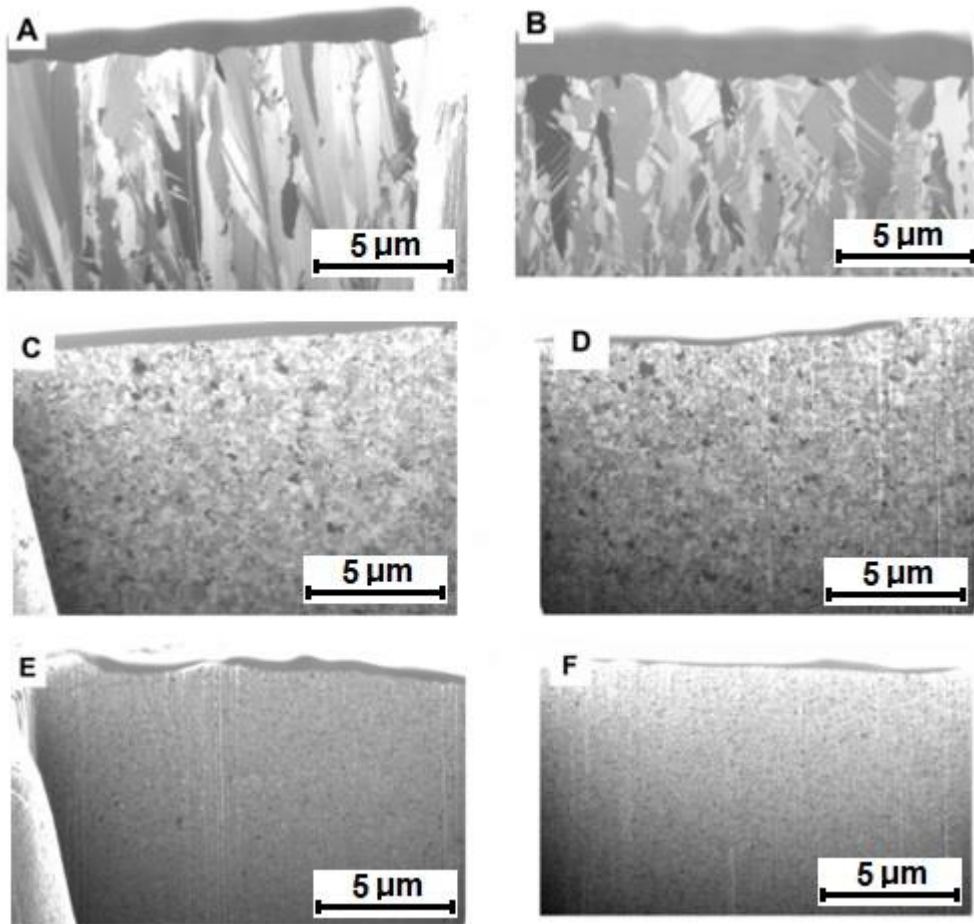


Fig 7.

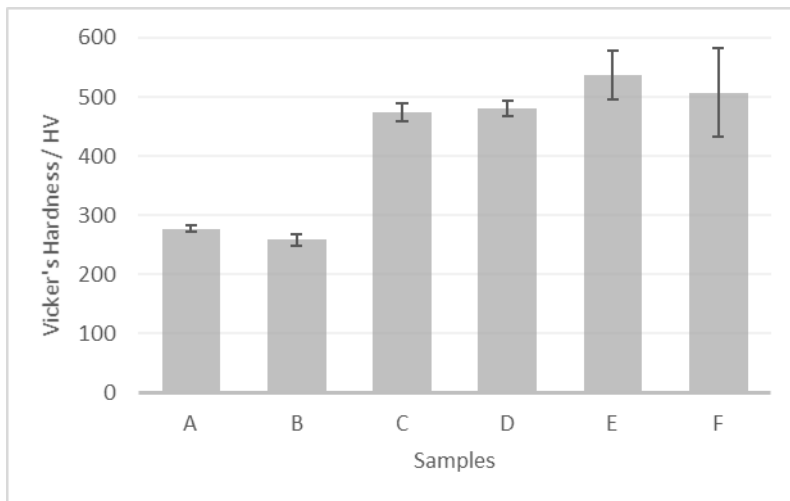


Fig 8.

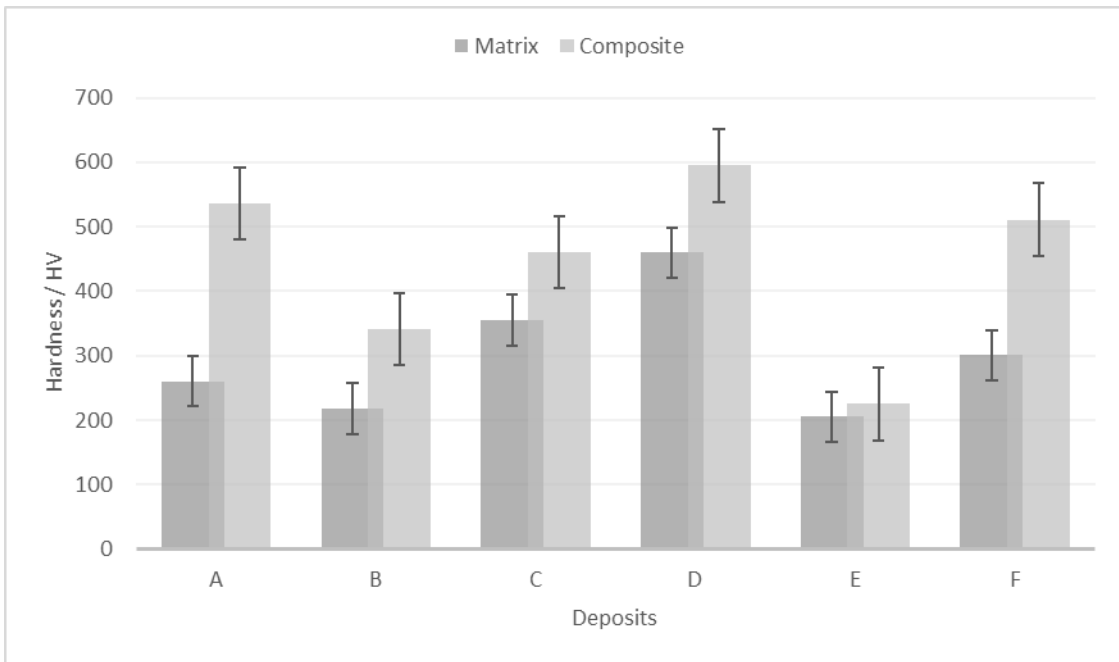


Fig 9.

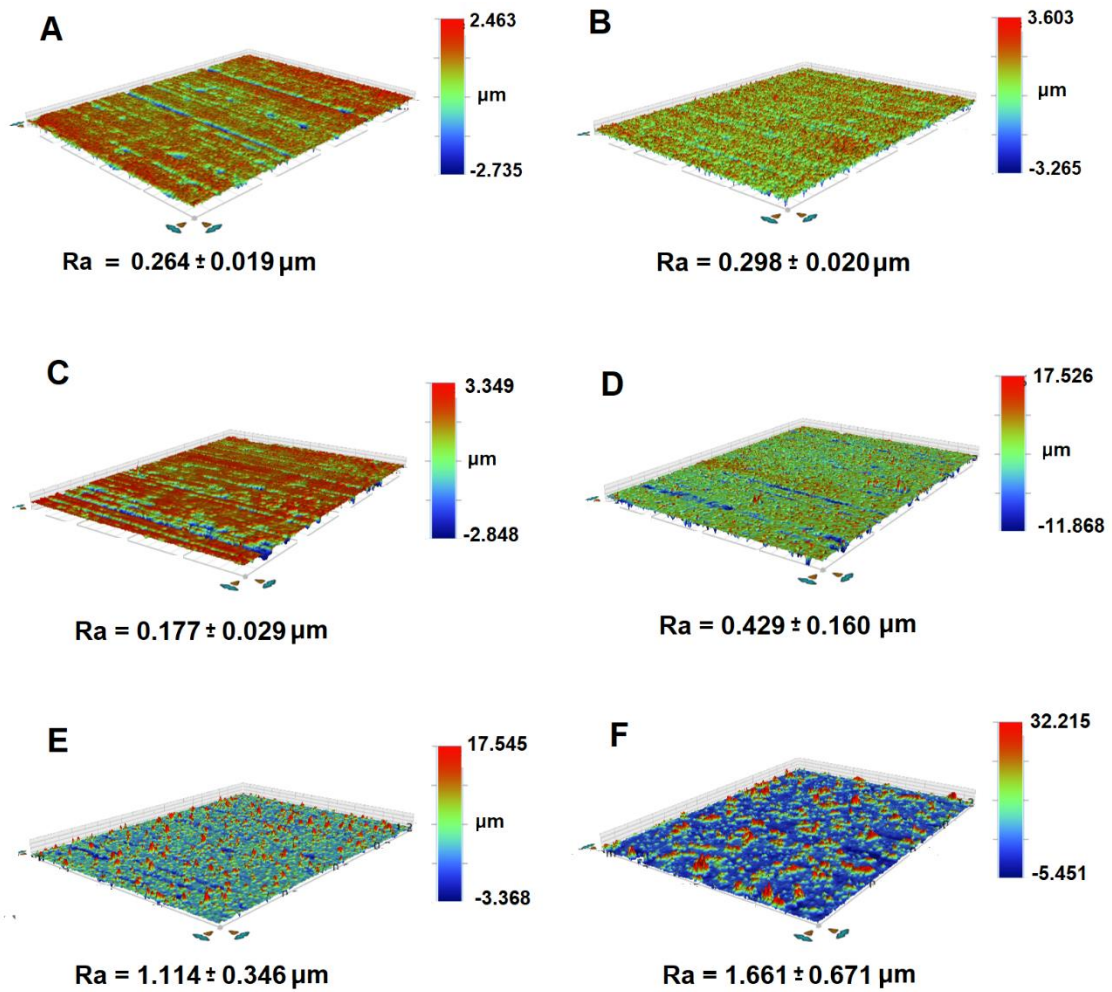


Fig 10.

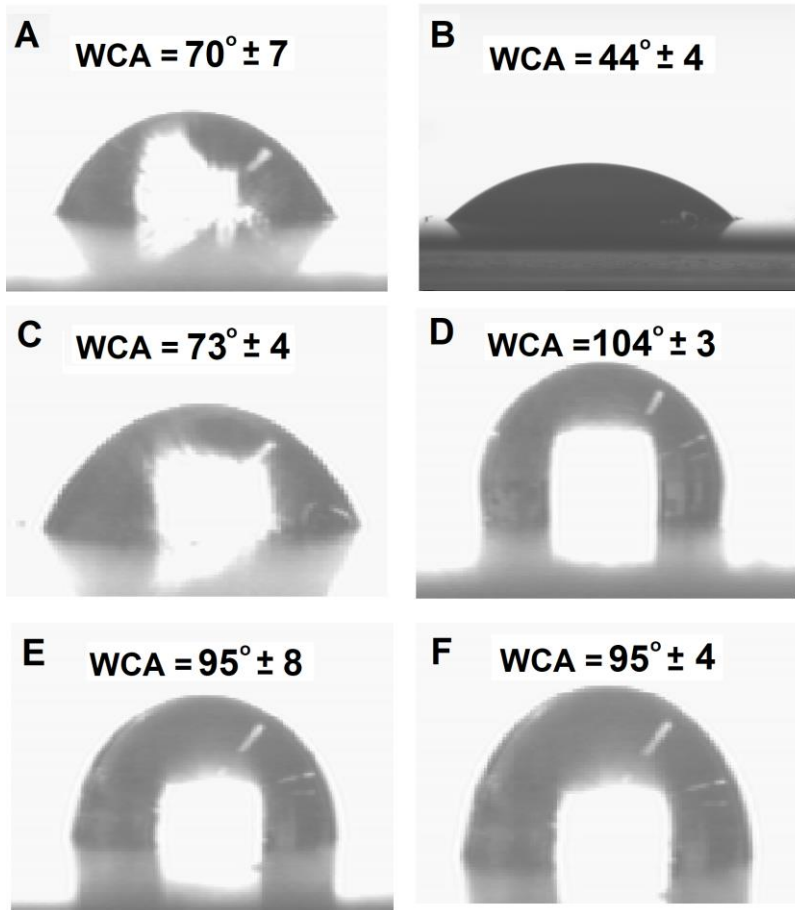


Fig 11.

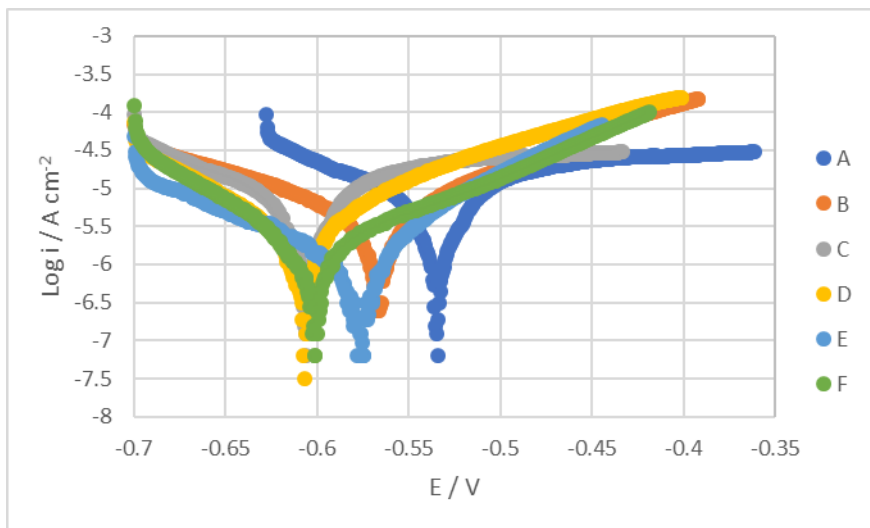


Fig 12.

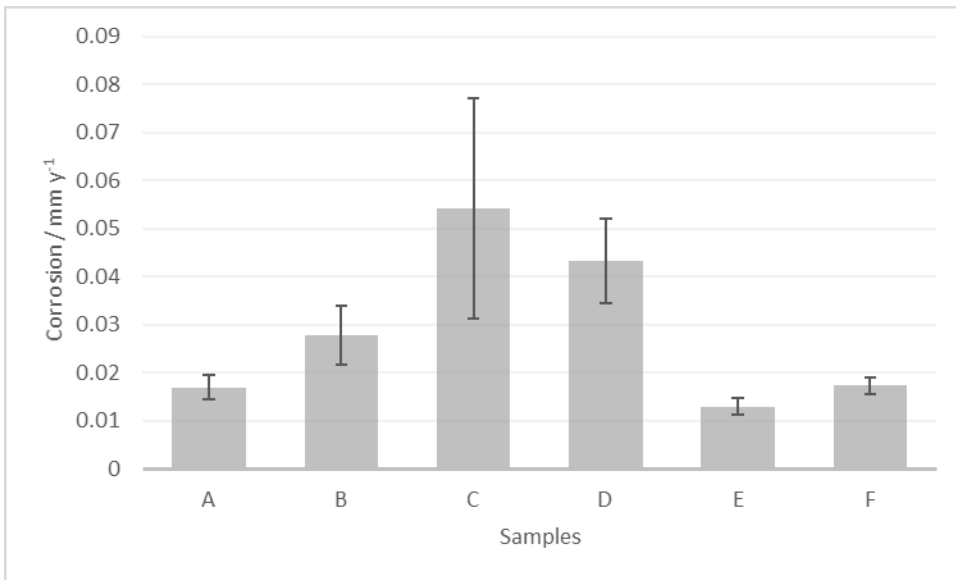


Fig 13.




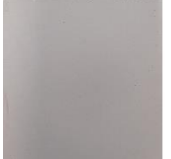



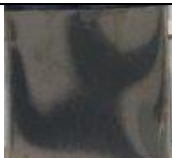










Samples	0 hours	24 hours	240 hours
A			
B			
C			
D			
E			
F			

Fig 14.

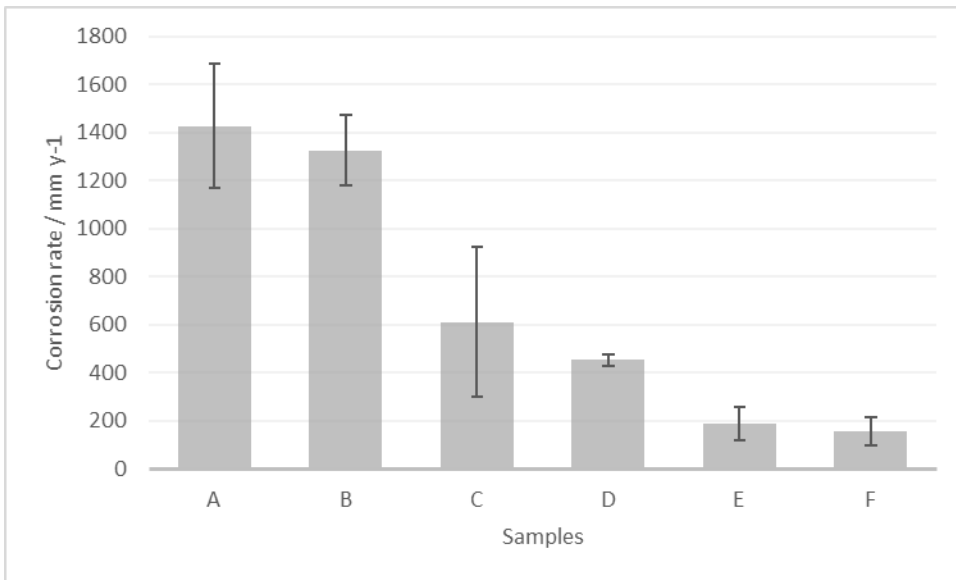


Fig 15.

Reference List

- [1] AZoM, Nickel (Ni) - Properties, Applications, 2018 (2001).
- [2] J. Sudagar, J. Lian, W. Sha, Electroless nickel, alloy, composite and nano coatings—A critical review, *J. Alloys Compounds*. 571 (2013) 183-204.
- [3] T. Borkar, S.P. Harimkar, Effect of electrodeposition conditions and reinforcement content on microstructure and tribological properties of nickel composite coatings, *Surf. Coat. Technol.* 205 (2011) 4124-4134.
- [4] Nickel institute, Plating: the role of nickel, 2019.
- [5] J. Chen, J. Li, D. Xiong, Y. He, Y. Ji, Y. Qin, Preparation and tribological behavior of Ni-graphene composite coating under room temperature, *Appl. Surf. Sci.* 361 (2016) 49-56.
- [6] L. Shi, C. Sun, P. Gao, F. Zhou, W. Liu, Electrodeposition and characterization of Ni–Co–carbon nanotubes composite coatings, *Surface and Coatings Technology*. 200 (2006) 4870-4875.
- [7] B. An, L. Li, H. Li, Electrodeposition in the Ni-plating bath containing multi-walled carbon nanotubes, *Mater. Chem. Phys.* 110 (2008) 481-485.
- [8] X. Chen, J. Peng, X. Li, F. Deng, J. Wang, W. Li, Tribological behavior of carbon nanotubes—reinforced nickel matrix composite coatings, *J. Mater. Sci. Lett.* 20 (2001) 2057-2060.
- [9] D. Iacovetta, J. Tam, U. Erb, Synthesis, structure, and properties of superhydrophobic nickel-PTFE nanocomposite coatings made by electrodeposition, *Surf. Coat. Technol.* 279 (2015) 134.
- [10] P. Dai, W. Xu, Q. Huang, Mechanical properties and microstructure of nanocrystalline nickel-carbon nanotube composites produced by electrodeposition, *Materials Science and Engineering: A*. 483 (2008) 172-174.
- [11] T. Lampke, A. Leopold, D. Dietrich, G. Alisch, B. Wielage, Correlation between structure and corrosion behaviour of nickel dispersion coatings containing ceramic particles of different sizes, *Surface and Coatings Technology*. 201 (2006) 3510-3517.
- [12] Y. Wu, H. Liu, B. Shen, L. Liu, W. Hu, The friction and wear of electroless Ni–P matrix with PTFE and/or SiC particles composite, *Tribol. Int.* 39 (2006) 553-559.
- [13] Z. Guo, R. Xu, X. Zhu, Studies on the wear resistance and the structure of electrodeposited RE-Ni-WP-SiC-PTFE composite materials, *Surface and Coatings Technology*. 187 (2004) 141-145.
- [14] K. Sung-Kyu, O. Tae-Sung, Electrodeposition behavior and characteristics of Ni-carbon nanotube composite coatings, *Transactions of Nonferrous Metals Society of China*. 21 (2011) s68-s72.

- [15] C. Carpenter, P. Shipway, Y. Zhu, The influence of CNT co-deposition on electrodeposit grain size and hardness, *Surface and Coatings Technology*. 205 (2011) 5059-5063.
- [16] M. Vaezi, S. Sadrnezhad, L. Nikzad, Electrodeposition of Ni–SiC nano-composite coatings and evaluation of wear and corrosion resistance and electroplating characteristics, *Colloids Surf. Physicochem. Eng. Aspects*. 315 (2008) 176-182.
- [17] C. Cai, X. Zhu, G. Zheng, Y. Yuan, X. Huang, F. Cao, J. Yang, Z. Zhang, Electrodeposition and characterization of nano-structured Ni–SiC composite films, *Surface and Coatings Technology*. 205 (2011) 3448-3454.
- [18] Y. Yang, R. Boom, B. Irion, D. van Heerden, P. Kuiper, H. de Wit, Recycling of composite materials, *Chemical Engineering and Processing: Process Intensification*. 51 (2012) 53-68.
- [19] McCormick science institute, *History of spices*, 2016.
- [20] Y. Hu, J. Zhang, W. Kong, G. Zhao, M. Yang, Mechanisms of antifungal and anti-aflatoxigenic properties of essential oil derived from turmeric (*Curcuma longa* L.) on *Aspergillus flavus*, *Food Chem*. 220 (2017) 1-8.
- [21] B.V. Chaitanya, K.V. Somisetty, A. Diwan, S. Pasha, N. Shetty, Y. Reddy, S. Nadigar, Comparison of Antibacterial Efficacy of Turmeric Extract, *Morinda Citrifolia* and 3% Sodium Hypochlorite on : An In-vitro Study, *Journal of clinical and diagnostic research : JCDR*. 10 (2016) ZC55.
- [22] J.S. Stanojević, L.P. Stanojević, D.J. Cvetković, B.R. Danilović, Chemical composition, antioxidant and antimicrobial activity of turmeric essential oil (*Curcuma longa* L.), *Advanced technologies*. 4 (2015) 19-25.
- [23] A.K. Tyagi, S. Prasad, W. Yuan, S. Li, B.B. Aggarwal, Identification of a novel compound (β -sesquiphellandrene) from turmeric (*Curcuma longa*) with anticancer potential: comparison with curcumin, *Invest. New Drugs*. 33 (2015) 1175.
- [24] M. Lechuga, M. Fernández-Serrano, E. Jurado, J. Núñez-Olea, F. Ríos, Acute toxicity of anionic and non-ionic surfactants to aquatic organisms, *Ecotoxicol. Environ. Saf*. 125 (2016) 1-8.
- [25] United States Department of Agriculture Agricultural Research Service, National Nutrient Database for Standard Reference Legacy Release, 02043, Spices, turmeric, ground. 2019 (2018).
- [26] M. Nagarnaik, A. Sarjoshi, A. Bodkhe, B. Khanal, M. Pise, G. Pandya, Characterization of active constituents in Turmeric powder and validation of method for curcumin in samples, *Asian Journal of Research in Chemistry*. 8 (2015) 643-647.
- [27] C.T. Rueden, J. Schindelin, M.C. Hiner, B.E. DeZonia, A.E. Walter, E.T. Arena, K.W. Eliceiri, ImageJ2: ImageJ for the next generation of scientific image data, *BMC Bioinformatics*. 18 (2017) 529.

- [28] M.A. Euterpio, C. Cavaliere, A.L. Capriotti, C. Crescenzi, Extending the applicability of pressurized hot water extraction to compounds exhibiting limited water solubility by pH control: curcumin from the turmeric rhizome, *Analytical and bioanalytical chemistry*. 401 (2011) 2977.
- [29] R. Zangi, B. Berne, Aggregation and dispersion of small hydrophobic particles in aqueous electrolyte solutions, *The Journal of Physical Chemistry B*. 110 (2006) 22736-22741.
- [30] R.A. French, A.R. Jacobson, B. Kim, S.L. Isley, R.L. Penn, P.C. Baveye, Influence of ionic strength, pH, and cation valence on aggregation kinetics of titanium dioxide nanoparticles, *Environ. Sci. Technol.* 43 (2009) 1354-1359.
- [31] D.J. McClements, S.R. Dungan, Factors that affect the rate of oil exchange between oil-in-water emulsion droplets stabilized by a nonionic surfactant: droplet size, surfactant concentration, and ionic strength, *J. Phys. Chem.* 97 (1993) 7304-7308.
- [32] E. Saka, C. Güler, The effects of electrolyte concentration, ion species and pH on the zeta potential and electrokinetic charge density of montmorillonite, *Clay Miner.* 41 (2006) 853-861.
- [33] R. Sprycha, Electrical double layer at alumina/electrolyte interface: I. Surface charge and zeta potential, *J. Colloid Interface Sci.* 127 (1989) 1-11.
- [34] V. Uskoković, R. Odsinada, S. Djordjevic, S. Habelitz, Dynamic light scattering and zeta potential of colloidal mixtures of amelogenin and hydroxyapatite in calcium and phosphate rich ionic milieus, *Arch. Oral Biol.* 56 (2011) 521-532.
- [35] J. Jiang, G. Oberdorster, P. Biswas, Characterization of size, surface charge, and agglomeration state of nanoparticle dispersions for toxicological studies.(Report), *Journal of Nanoparticle Research: An Interdisciplinary Forum for Nanoscale Science and Technology*. 11 (2009) 77.
- [36] I. Tudela, Y. Zhang, M. Pal, I. Kerr, T.J. Mason, A.J. Cobley, Ultrasound-assisted electrodeposition of nickel: Effect of ultrasonic power on the characteristics of thin coatings, *Surface and Coatings Technology*. 264 (2015) 49-59.
- [37] S. Ghosh, P. Limaye, B. Swain, N. Soni, R. Agrawal, R. Dusane, A. Grover, Tribological behaviour and residual stress of electrodeposited Ni/Cu multilayer films on stainless steel substrate, *Surface and Coatings Technology*. 201 (2007) 4609-4618.
- [38] Nickel institute, *Nickel Plating Handbook*, Nickel institute, Brussels, 2014.
- [39] T.M. Chang, M. Sone, A. Shibata, C. Ishiyama, Y. Higo, Bright nickel film deposited by supercritical carbon dioxide emulsion using additive-free Watts bath, *Electrochim. Acta*. 55 (2010) 6469-6475.
- [40] A. Rashidi, A. Amadeh, The effect of saccharin addition and bath temperature on the grain size of nanocrystalline nickel coatings, *Surface and Coatings Technology*. 204 (2009) 353-358.

- [41] A. Fahami, B. Nasiri-Tabrizi, M. Rostami, R. Ebrahimi-Kahrizsangi, Influence of surfactants on the Characteristics of Nickel Matrix Nanocomposite Coatings, *ISRN Electrochemistry*. (2013) 1-8.
- [42] A. Wang, B. Chen, L. Fang, J. Yu, L. Wang, Influence of branched quaternary ammonium surfactant molecules as levelers for copper electroplating from acidic sulfate bath, *Electrochim. Acta*. 108 (2013) 698-706.
- [43] M.A. Malik, M.A. Hashim, F. Nabi, S.A. Al-Thabaiti, Z. Khan, Anti-corrosion ability of surfactants: a review, *Int.J.Electrochem.Sci*. 6 (2011) 1927-1948.
- [44] R. Vittal, H. Gomathi, K. Kim, Beneficial role of surfactants in electrochemistry and in the modification of electrodes, *Adv. Colloid Interface Sci*. 119 (2006) 55-68.
- [45] V. Darrort, M. Troyon, J. Ebothé, C. Bissieux, C. Nicollin, Quantitative study by atomic force microscopy and spectrophotometry of the roughness and brightness of electrodeposited nickel in the presence of additives, *Thin Solid Films*. 265 (1995) 52-57.
- [46] E. Saubestre, The Chemistry of bright Nickel plating solutions, *Plating*. 45 (1958) 1219-1227.
- [47] H. Alimadadi, M. Ahmadi, M. Aliofkhazraei, S.R. Younesi, Corrosion properties of electrodeposited nanocrystalline and amorphous patterned Ni–W alloy, *Mater Des*. 30 (2009) 1356-1361.
- [48] F. C. Walsh* C. Ponce de Leon., A review of the electrodeposition of metal matrix composite coatings by inclusion of particles in a metal layer: an established and diversifying technology, *Transactions of the IMF*. 92 (2014) 83-98.
- [49] V. Medeliene, A. Kosenko, Structural and functional properties of electrodeposited copper metal matrix composite coating with inclusions of WC, *Mater.Sci*. 14 (2008) 29-33.
- [50] K. Rajkumar, S. Aravindan, Tribological studies on microwave sintered copper–carbon nanotube composites, *Wear*. 270 (2011) 613-621.
- [51] Y. Yang, Y. Wang, Y. Ren, C. He, J. Deng, J. Nan, J. Chen, L. Zuo, Single-walled carbon nanotube-reinforced copper composite coatings prepared by electrodeposition under ultrasonic field, *Mater Lett*. 62 (2008) 47-50.
- [52] S. Spanou, E. Pavlatou, N. Spyrellis, Ni/nano-TiO₂ composite electrodeposits: Textural and structural modifications, *Electrochim. Acta*. 54 (2009) 2547-2555.
- [53] J. Amblard, M. Froment, G. Maurin, N. Spyrellis, A method of preparing cross sectioned vertically thin foils-description of the various types of fibers in nickel electro-deposits, *Journal de microscopie et de spectroscopie électroniques*. 6 (1981) 311.
- [54] J. Amblard, M. Froment, N. Spyrellis, Origine des textures dans les depots électrolytiques de nickel, *Surface Technology*. 5 (1977) 205-234.

- [55] J. Amblard, I. Epelboin, M. Froment, G. Maurin, Inhibition and nickel electrocrystallization, *J. Appl. Electrochem.* 9 (1979) 233-242.
- [56] H. Karayannis, G. Paternarakis, Effect of the Cl⁻ and SO₄²⁻ ions on the selective orientation and structure of Ni electrodeposits, *Electrochim. Acta.* 40 (1995) 1079-1092.
- [57] A. Engwall, Z. Rao, E. Chason, Origins of residual stress in thin films: Interaction between microstructure and growth kinetics, *Mater Des.* 110 (2016) 616-623.
- [58] J. Kubisztal, A. Budniok, A. Lasia, Study of the hydrogen evolution reaction on nickel-based composite coatings containing molybdenum powder, *Int J Hydrogen Energy.* 32 (2007) 1211-1218.
- [59] Y. Song, D. Shan, R. Chen, E. Han, A novel dual nickel coating on AZ91D magnesium alloy, *Transactions of Nonferrous Metals Society of China.* 18 (2008) s339-s343.
- [60] D. Suarez, F. Olson, Nodulation of electrodeposited copper in the presence of thiourea, *J. Appl. Electrochem.* 22 (1992) 1002-1010.
- [61] T. Andersen, C. Pitt, L. Livingston, Nodulation of electrodeposited copper due to suspended particulate, *J. Appl. Electrochem.* 13 (1983) 429-438.
- [62] Q. Zhang, Y. Liu, Y. Liu, Y. Ren, Y. Wu, Z. Gao, X. Wu, P. Han, Enhanced tensile ductility and strength of electrodeposited ultrafine-grained nickel with a desired bimodal microstructure, *Materials Science and Engineering: A.* 701 (2017) 196-202.
- [63] C. Guo, Y. Zuo, X. Zhao, J. Zhao, J. Xiong, Effects of surfactants on electrodeposition of nickel-carbon nanotubes composite coatings, *Surface and Coatings Technology.* 202 (2008) 3385-3390.
- [64] C. Low, R. Wills, F. Walsh, Electrodeposition of composite coatings containing nanoparticles in a metal deposit, *Surface and Coatings Technology.* 201 (2006) 371-383.
- [65] H. Gül, F. Kılıç, M. Uysal, S. Aslan, A. Alp, H. Akbulut, Effect of particle concentration on the structure and tribological properties of submicron particle SiC reinforced Ni metal matrix composite (MMC) coatings produced by electrodeposition, *Appl. Surf. Sci.* 258 (2012) 4260-4267.
- [66] N. Elkhoshkhany, A. Hafnway, A. Khaled, Electrodeposition and corrosion behavior of nano-structured Ni-WC and Ni-Co-WC composite coating, *J. Alloys Compounds.* 695 (2017) 1505-1514.
- [67] M. Surender, B. Basu, R. Balasubramaniam, Wear characterization of electrodeposited Ni-WC composite coatings, *Tribol. Int.* 37 (2004) 743-749.
- [68] C. Zanella, M. Lekka, P. Bonora, Effect of ultrasound vibration during electrodeposition of Ni-SiC nanocomposite coatings, *Surface Engineering.* (2013).

- [69] S. Khabazian, S. Sanjabi, The effect of multi-walled carbon nanotube pretreatments on the electrodeposition of Ni–MWCNTs coatings, *Appl. Surf. Sci.* 257 (2011) 5850-5856.
- [70] S. Mirzamohammadi, H. Khorsand, M. Aliofkhaeaei, Effect of different organic solvents on electrodeposition and wear behavior of Ni-alumina nanocomposite coatings, *Surface and Coatings Technology*. 313 (2017) 202-213.
- [71] P. Indyka, E. Beltowska-Lehman, M. Bieda, J. Morgiel, L. Tarkowski, Microstructure and Deposition Relations in Alumina Particle Strengthened Ni-W Matrix Composites, 186 (2012) 234-238.
- [72] E. García-Lecina, I. García-Urrutia, J.A. Díez, J. Morgiel, P. Indyka, A comparative study of the effect of mechanical and ultrasound agitation on the properties of electrodeposited Ni/ Al₂O₃ nanocomposite coatings, *Surf. Coat. Technol.* 206 (2012) 2998-3005.
- [73] E. Beltowska-Lehman, P. Indyka, A. Bigos, M. Kot, L. Tarkowski, Electrodeposition of nanocrystalline Ni–W coatings strengthened by ultrafine alumina particles, *Surface and Coatings Technology*. 211 (2012) 62-66.
- [74] Q. Zhang, Y. Liu, Y. Liu, Y. Ren, Y. Wu, Z. Gao, X. Wu, P. Han, Enhanced tensile ductility and strength of electrodeposited ultrafine-grained nickel with a desired bimodal microstructure, *Materials Science & Engineering A; Materials Science & Engineering A*. 701 (2017) 196-202.
- [75] J. Lohmiller, M. Greuer, C. Braun, A. Kobler, C. Kübel, K. Schüller, V. Honkimäki, H. Hahn, O. Kraft, R. Birringer, P.A. Gruber, Untangling dislocation and grain boundary mediated plasticity in nanocrystalline nickel, *Acta Materialia*. 65 (2014) 295-307.
- [76] K. Schüller, B. Philippi, M. Weinmann, V.M. Marx, H. Vehoff, Effects of processing on texture, internal stresses and mechanical properties during the pulsed electrodeposition of nanocrystalline and ultrafine-grained nickel, *Acta Materialia*. 61 (2013) 3945-3955.
- [77] R. Mishra, B. Basu, R. Balasubramaniam, Effect of grain size on the tribological behavior of nanocrystalline nickel, *Materials Science and Engineering: A*. 373 (2004) 370-373.
- [78] J. Schiøtz, F.D. Di Tolla, K.W. Jacobsen, Softening of nanocrystalline metals at very small grain sizes, *Nature*. 391 (1998) 561.
- [79] N. Krasilnikov, W. Lojkowski, Z. Pakiel, R. Valiev, Tensile strength and ductility of ultra-fine-grained nickel processed by severe plastic deformation, *Materials Science and Engineering: A*. 397 (2005) 330-337.
- [80] G. Hughes, S. Smith, C. Pande, H. Johnson, R. Armstrong, Hall-Petch strengthening for the microhardness of twelve nanometer grain diameter electrodeposited nickel, *Scripta Metallurgica*. 20 (1986) 93-97.

- [81] Z. Ren, N. Meng, K. Shehzad, Y. Xu, S. Qu, B. Yu, J. Luo, Mechanical properties of nickel-graphene composites synthesized by electrochemical deposition, *Nanotechnology*. 26 (2015) 065706.
- [82] N. Hansen, Hall–Petch relation and boundary strengthening, *Scr. Mater.* 51 (2004) 801-806.
- [83] E.O. Hall, *Proc Phys Soc London B*. 64 (1951).
- [84] N.J. Petch, *J Iron Steel Inst.* 174 (1953).
- [85] K.C. Ludema, A review of scuffing and running-in of lubricated surfaces, with asperities and oxides in perspective, *Wear*. 100 (1984) 315-331.
- [86] M. Rapetto, A. Almqvist, R. Larsson, P. Lugt, On the influence of surface roughness on real area of contact in normal, dry, friction free, rough contact by using a neural network, *Wear*. 266 (2009) 592-595.
- [87] D. Janssen, R. De Palma, S. Verlaak, P. Heremans, W. Dehaen, Static solvent contact angle measurements, surface free energy and wettability determination of various self-assembled monolayers on silicon dioxide, *Thin Solid Films*. 515 (2006) 1433-1438.
- [88] D.E. Packham, Surface energy, surface topography and adhesion, *Int J Adhes Adhes.* 23 (2003) 437-448.
- [89] L. Vitos, A. Ruban, H.L. Skriver, J. Kollar, The surface energy of metals, *Surf. Sci.* 411 (1998) 186-202.
- [90] M. McLean, Determination of the surface energy of copper as a function of crystallographic orientation and temperature, *Acta Metallurgica*. 19 (1971) 387-393.
- [91] R.N. Wenzel, Surface roughness and contact angle. *J. Phys. Chem.* 53 (1949) 1466-1467.
- [92] A. Cassie, S. Baxter, Wettability of porous surfaces, *Transactions of the Faraday society*. 40 (1944) 546-551.
- [93] L. Bonin, V. Vitry, F. Delaunois, Corrosion behaviour of electroless high boron-mid phosphorous nickel duplex coatings in the as-plated and heat-treated states in NaCl, H₂SO₄, NaOH and Na₂SO₄ media, *Mater. Chem. Phys.* 208 (2018) 77-84.
- [94] P. Agarwal, D. Landolt, Effect of anions on the efficiency of aromatic carboxylic acid corrosion inhibitors in near neutral media: Experimental investigation and theoretical modeling, *Corros. Sci.* 40 (1998) 673-691.
- [95] J. Popplewell, R. Hart, J. Ford, The effect of iron on the corrosion characteristics of 90-10 cupro nickel in quiescent 3- 4% NaCl solution, *Corros. Sci.* 13 (1973) 295-309.
- [96] F. Nasirpouri, M.R. Sanaeian, A.S. Samardak, E.V. Sukovatitsina, A.V. Ognev, L.A. Chebotkevich, M.-. Hosseini, M. Abdolmaleki, An investigation on the effect of

surface morphology and crystalline texture on corrosion behavior, structural and magnetic properties of electrodeposited nanocrystalline nickel films, *Appl. Surf. Sci.* 292 (2014) 795-805.

[97] A. El-Sayed, H. Mohran, H. Abd El-Lateef, Corrosion Study of Zinc, Nickel, and Zinc-Nickel Alloys in Alkaline Solutions by Tafel Plot and Impedance Techniques, *Metallurgical and Materials Transactions*. 43 (2012) 619-632.

[98] B. Rosborg, J. Pan, C. Leygraf, Tafel slopes used in monitoring of copper corrosion in a bentonite/groundwater environment, *Corros. Sci.* 47 (2005) 3267-3279.

[99] G. Instruments, *Getting Started with Electrochemical Corrosion Measurement*. (2011).

[100] E. Beltowska-Lehman, P. Indyka, A. Bigos, M. Kot, L. Tarkowski, Electrodeposition of nanocrystalline Ni–W coatings strengthened by ultrafine alumina particles, *Surface and Coatings Technology*. 211 (2012) 62-66.